Available online at www.sciencedirect.com
ScienceDirect
Trans. Nonferrous Met. Soc. China 28(2018) 1801−1807
Transactions of Nonferrous Metals Society of China
www.tnmsc.cn

Sol−gel auto-combustion synthesis of $K_xNa_{1-x}NbO_3$ nanopowders and ceramics: Dielectric and piezoelectric properties

Hua-lei CHENG[1,2], Jian XIAO[1], Peng GAO[1], Yun-yun YAN[1], Shuan-ping GAO[1], Hong-liang DU[2,3]

1. Key Laboratory of Phytochemistry of Shaanxi Province, College of Chemistry and Chemical Engineering, Baoji University of Arts and Sciences, Baoji 721013, China;
2. State Key Laboratory of Solidification Processing, School of Materials Science and Engineering Northwestern Polytechnical University, Xi'an 710072, China;
3. Science College, Air Force Engineering University, Xi'an 710051, China

Received 17 May 2017; accepted 27 October 2017

Abstract: The $K_xNa_{1-x}NbO_3$ nanopowders with cubic-like morphology and an average size of about 50 nm were synthesized by sol−gel auto-combustion method. And then, the ceramics were prepared and the phase transition, microstructure and electrical properties of the $K_xNa_{1-x}NbO_3$ ceramics were investigated. Pure perovskite phases of the $K_xNa_{1-x}NbO_3$ ceramics were confirmed by XRD patterns and the $K_{0.50}Na_{0.50}NbO_3$ ceramics show the coexistence of orthorhombic and monoclinic structures. SEM micrographs show that all samples have bimodal grain size distributions and the number of the small grains decrease with increasing K^+ content in the bimodal grain size distribution system. The $K_{0.50}Na_{0.50}NbO_3$ ceramics with the uniform grain size and the maximum density show excellent electrical properties with ε_r=467.40, tan δ=0.020, d_{33}=128 pC/N and k_p=0.32 at the room temperature, demonstrating that the properties of the $K_{0.50}Na_{0.50}NbO_3$ powers prepared by sol−gel auto-combustion are excellent and the ceramics are promising lead-free piezoelectric materials.

Key words: sol−gel auto-combustion; $K_xNa_{1-x}NbO_3$; phase transition; microstructure; electrical properties

1 Introduction

From the viewpoint of sustainable development of the world, lead-free ceramics have received considerable attention [1]. Lead-free $K_{0.5}Na_{0.5}NbO_3$(KNN)-based ceramics have been considered as a good candidate for lead-free piezoelectric ceramics because of their strong piezoelectricity and high Curie temperature [2]. However, a major problem concerning this material is its poor sinterability [3]. The improved density and higher d_{33} values of the KNN ceramics have been obtained by hot pressing or spark plasma sintering [4,5]. However, these ways could not be adapted to industrial production because of high cost. Another method is suppressing the loss of alkali metals or the formation of liquid phases by doping with the second phase [6−10]. However, the selectivity of the second phase and the processing parameters are complicated.

Contrary to the conventional solid state reaction (CSSR) method, the wet chemical routes become the excellent techniques for the synthesis of high-purity multi-component oxides [11]. It has been confirmed that the chemical methods like chemical co-precipitation [12], sol−gel technique [13], hydrothermal [14,15], microemulsion mediated syntheses [16,17], and molten-salt method [18] can control the morphology and the chemical compositions of the prepared powder very efficiently. These methods increase the homogeneity and surface area of the resulting powders which lead to relatively high activity and hence low sintering temperature. Compared with these methods, the sol−gel auto-combustion method is one of the most promising techniques because of its cheaper precursors, simple route of preparation, lower heat-treated temperature and achievement of ultrafine and homogeneous multi-

Foundation item: Project (21501007) supported by the National Natural Science Foundation of China; Project (2016GY-226) supported by the Industrial Science and Technology Plan in Shaanxi Province of China; Project (ZK15044) supported by the Doctoral Scientific Research Starting Foundation of Baoji University of Arts and Sciences, China; Project (201610721039) supported by Undergraduate Training Programs for Innovation and Entrepreneurship, China

Corresponding author: Hua-lei CHENG; Tel: +86-15771696066; E-mail: hualeicheng@163.com

DOI: 10.1016/S1003-6326(18)64824-1

component powders. In this work, the $K_xNa_{1-x}NbO_3$ powders were synthesized by the citric acid-assisted sol−gel auto-combustion method and then pressed into disks and the phase transition, microstructure and electrical properties of the samples were systematically investigated.

2 Experimental

All the chemicals used in this reaction were analytical grade and the schematic diagram is shown in Fig. 1. A niobium precursor solution was prepared firstly from Nb_2O_5 (99.9%) and KOH (95%). The powders were mixed thoroughly and heated at 350 °C for 2 h to obtain water-soluble K_3NbO_4 which was then dissolved in distilled water and titrated with oxalic acid to form a $K_4Nb_6O_{19}$ precipitate. After removal of the residual K^+, the precipitate was chelated with citric acid to form the niobium precursor solution. And then, stoichiometric amounts of KNO_3 and $NaNO_3$ were weighed according to the formula of $K_xNa_{1-x}NbO_3$ and dissolved in a mixture of the niobium precursor solution. The mixed citrate−nitrate aqueous solution was continuously stirred for 4 h and concentrated by evaporation at 80 °C, producing a transparent gel and then ignited at any point. The as-burnt powders were pressed into disks of 12 mm in diameter and 1 mm in thickness under 300 MPa using polyvinyl alcohol (PVA) as a binder. After burning off PVA, the pellets were sintered at 1100 °C for 2 h in the sealed Al_2O_3 crucibles. The obtained samples were polished. Silver paste was fired on both sides of the samples at 810 °C for 20 min as the electrodes for the sake of measurements.

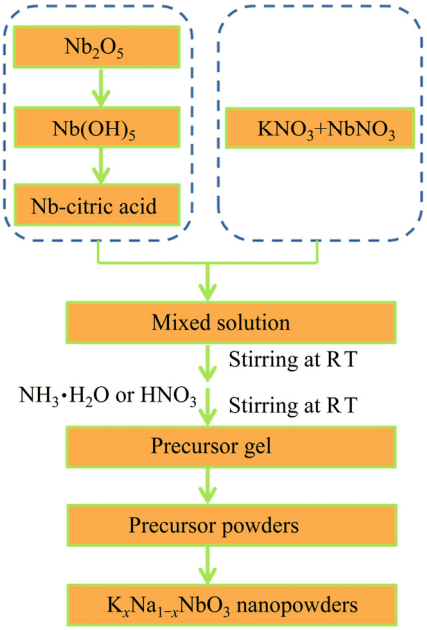

Fig. 1 Schematic diagram of synthesis of $K_xNa_{1-x}NbO_3$ nano-powders by sol−gel auto-combustion

The Fourier transform infrared (FT-IR) spectroscopic measurements were made using an IR spectrophotometer (Perkinelmer Frontier, America). The phase structures were examined using X-ray powder diffraction analysis with a Cu K_α radiation (Philips X-Pert ProDiffractometer, Almelo, and The Netherlands) at room temperature. The microstructure evolution was observed using a scanning electron microscopy (Model JSM−6360, JEOL, Tokyo, Japan). The dielectric spectrum measurements were performed using the LCR meter (Agilent E4980, USA). The piezoelectric constant (d_{33}) was measured using a piezo-d_{33} meter (ZJ−3A, Institute of Acoustics Academic Sinica, Beijing, China). The planar electromechanical coupling factor k_p was calculated by the resonance−antiresonance method on the basis of IEEE standards using an impedance analyzer (Agilent 4294A).

3 Results and discussion

3.1 Powders characterization

The chemical and structural changes of the dried gels and the as-burnt powders of $K_xNa_{1-x}NbO_3$ can be observed from the IR spectra (Fig. 2). The dried gels show two absorption bands at about 1620 and 1380 cm^{-1} corresponding to the carboxyl group and NO^{3-} ion, respectively [19]. After the auto-combustion, the

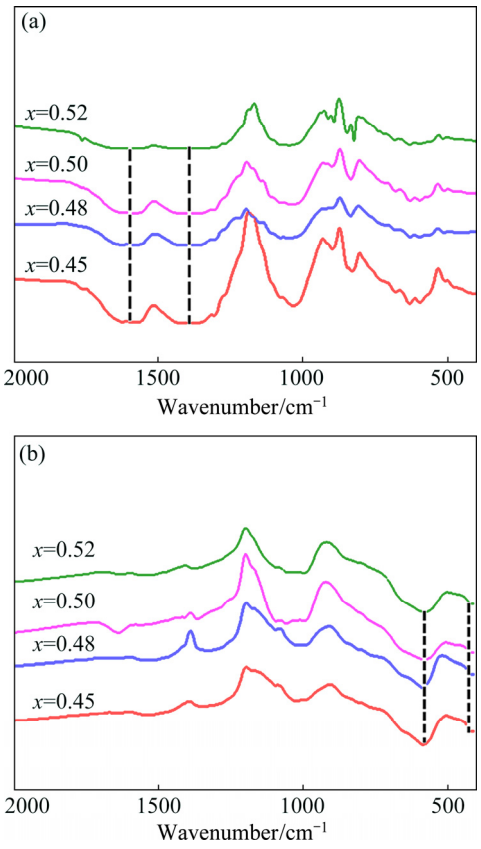

Fig. 2 IR spectra of dried gels (a) and as-burnt powders (b) for $K_xNa_{1-x}NbO_3$

intensities of the absorption bands at about 1620 and 1380 cm^{-1} reduce and two new strong absorption bands appear in the range of 600−400 cm^{-1}. The reduction of the two bands indicates the reaction between carboxyl groups and NO^{3-} ions during the auto-combustion process.

Figure 3 shows the XRD patterns of the $K_xNa_{1-x}NbO_3$ nano-powders. It can be seen that all the compositions can be indexed by perovskite structure symmetry, and no secondary phase is observed. It is also noted that the diffraction peaks shift slightly towards lower diffraction angles as x increases. This may be attributed to the larger ionic radius of K^+ as compared to Na^+. Because the radius of K^+ (0.164 nm) is larger than that of Na^+ (0.139 nm), the larger number of K^+ leads to the larger distance of the crystal face, and as a result, the 2θ of $K_xNa_{1-x}NbO_3$ patterns decreases. It needs several hours to prepare the single phase $K_xNa_{1-x}NbO_3$ powders by solid state reaction route at ~850 °C, whereas the sol−gel auto-combustion process just takes a few minutes at room temperature. The reason is that a strong redox reaction is completed in a short time, which shows relatively high activity and hence lowers the processing temperature and increases the homogeneity and surface area of the resulting powders.

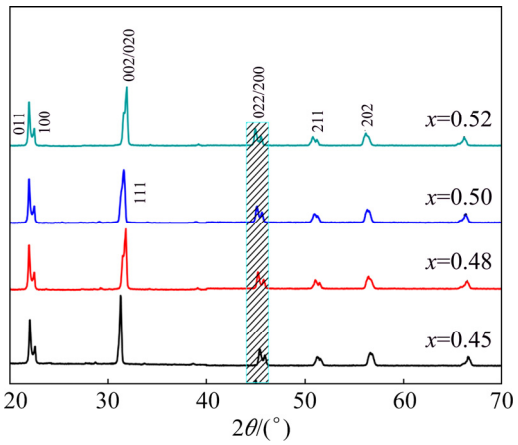

Fig. 3 XRD patterns of $K_xNa_{1-x}NbO_3$ nano-powders

Figure 4 shows the FE-SEM images of the $K_{0.5}Na_{0.5}NbO_3$ as-burnt powders. Obviously, the powders show porous three-dimension structure, as shown in Fig. 4(a). The porous microstructure is a characteristic for the sol−gel auto-combustion powders. For the sol−gel auto-combustion process, the organic materials decompose and the strong redox reactions are completed in a short time. These reactions release a lot of gas to promote the pores forming. In Fig. 4(b), the shape of $K_{0.5}Na_{0.5}NbO_3$ particles is tended to be cubic morphology and the size distribution is rather uniform, and the average size of the powders is about 50 nm, demonstrating that the sol−gel auto-combustion method is a promising technique to prepare the $K_{0.50}Na_{0.50}NbO_3$ powers with controllable morphology.

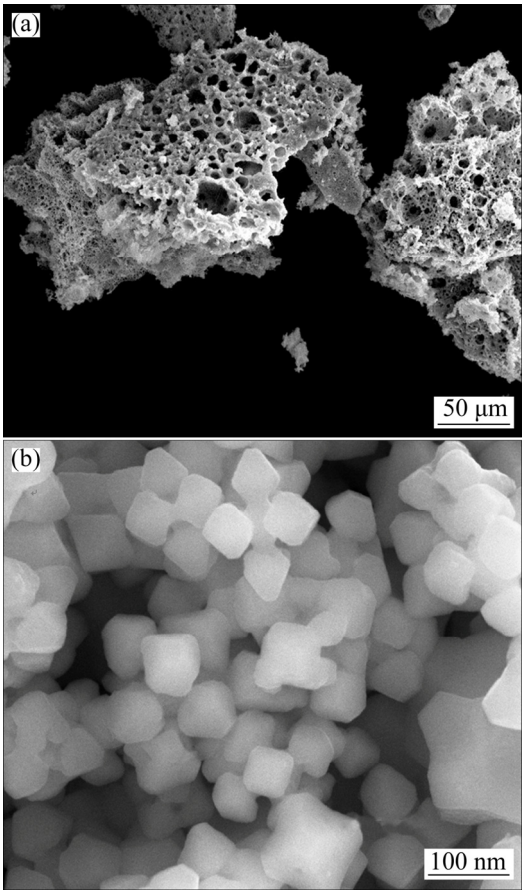

Fig. 4 FE-SEM images of $K_{0.5}Na_{0.5}NbO_3$ nano-powders after combustion

3.2 Ceramics characterization

Figure 5 shows the XRD patterns of $K_xNa_{1-x}NbO_3$ ceramics. According to Fig. 5 and characteristic X-ray diffraction patterns for various symmetries, it can be

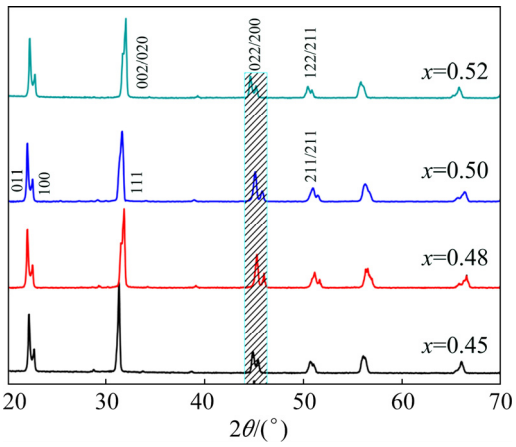

Fig. 5 XRD patterns of $K_xNa_{1-x}NbO_3$ ceramics

concluded that the phase structures of the compositions corresponding to $x \leq 0.48$ and $x=0.52$ exhibit monoclinic and orthorhombic structures, respectively. Whereas, the coexistence of orthorhombic and monoclinic structures is found in the composition corresponding to $x=0.50$ near the 50/50 morphotropic phase boundary (MPB) region. The lattice parameters of the $K_xNa_{1-x}NbO_3$ ceramics determined by the GwBasic software are given in Table 1. The existence of double structures in $K_{0.50}Na_{0.50}NbO_3$ confirms the MPB nature, which is consistent with the previous report [20].

Table 1 Lattice parameters of $K_xNa_{1-x}NbO_3$ ceramics

x	a/Å	b/Å	c/Å	Structure
0.45	3.987	3.938	3.979	Monoclinic
0.48	4.132	4.034	7.354	Monoclinic
0.50	5.672	5.642	3.944	Monoclinic
	5.639	5.672	3.944	Orthorhombic
0.52	3.926	8.118	6.045	Orthorhombic

Figure 6 shows SEM images of the $K_xNa_{1-x}NbO_3$ ceramics. Dense surface microstructures with bimodal grain size distributions are observed for all samples. The bimodal grain size distribution shows square/rectangular shaped grains. The bimodal grain size distributions are caused by the presence of liquid phase, but we did not find the liquid phase in our samples. In additional, the number of the small grains decreases with increasing K^+ content in the bimodal grain size distributions system. The grain boundary of the ceramics becomes clear and the porosity of the samples decreases. The $K_{0.5}Na_{0.5}NbO_3$ ceramics have clear grain boundary and the grain size is about 5 μm.

Figure 7 shows the variations of bulk density and relative density of the $K_xNa_{1-x}NbO_3$ ceramics. The bulk densities of the $K_xNa_{1-x}NbO_3$ systems were measured using the Archimedes' principle. The theoretical relative densities for these KNN ceramics were calculated using the measured mass densities and the lattice parameter data obtained from the XRD analysis described in Table 1. It is found that the bulk densities of the $K_xNa_{1-x}NbO_3$ ceramics increase and then decrease with increasing the K^+ content. The maximum density is found in the $K_{0.50}Na_{0.50}NbO_3$ compositions. The theoretical relative densities show the similar tendency and the values are between 94.9% and 97.5%. The densities increase with the increase in K^+ content of KNN system, which suggests that excessive K^+ ions cause liquid phase sintering and hence lead to the increased densities. Therefore, K^+ ions act as sintering aid in KNN system [21]. When $x>0.5$, the density decreases with the further increase of K^+ content. This can be explained on the basis of increasing the volatilization with further increase of K^+ in the compositions near the MPBs [22]. The densities of the $K_xNa_{1-x}NbO_3$ ceramics are consistent with the SEM images.

Figure 8 shows the temperature dependence of dielectric permittivity and dielectric loss at 10 kHz for

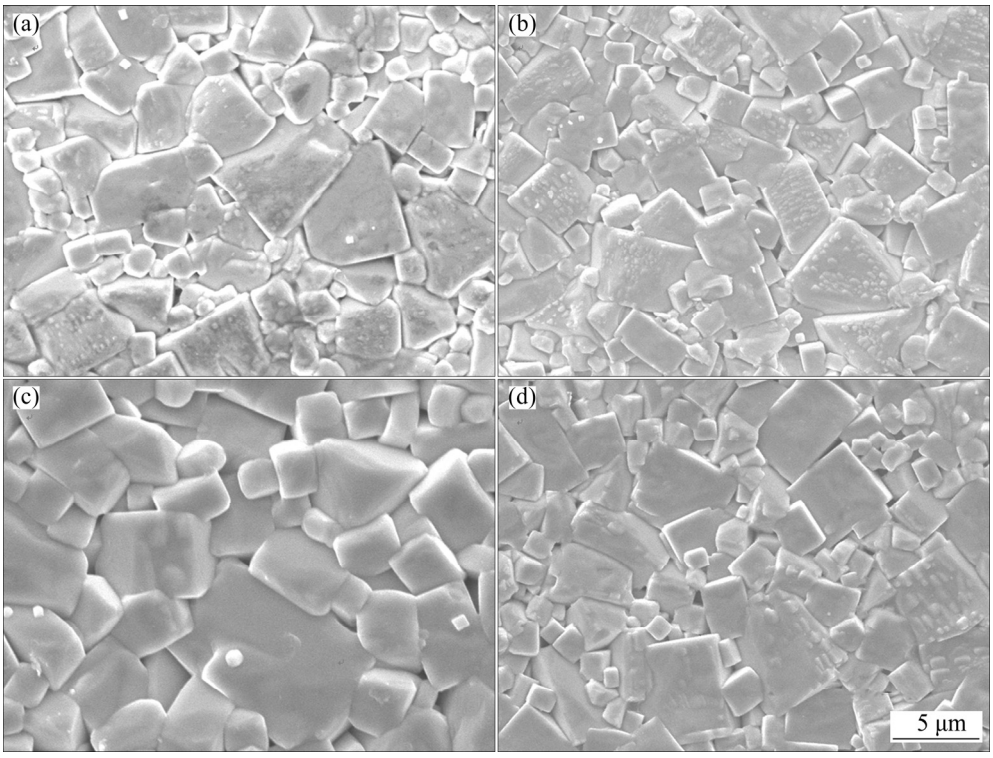

Fig. 6 SEM images of $K_xNa_{1-x}NbO_3$ ceramics: (a) $x=0.45$; (b) $x=0.48$; (c) $x=0.50$; (d) $x=0.52$

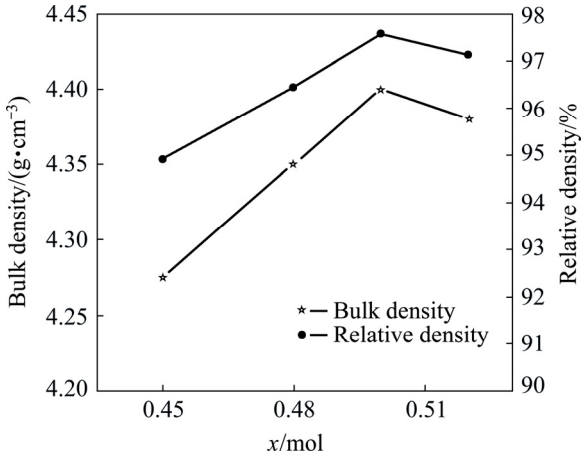

Fig. 7 Variations of bulk density and relative density of $K_xNa_{1-x}NbO_3$ ceramics

$K_xNa_{1-x}NbO_3$ ceramics. It is evident from Fig. 8(a) that different compositions of $K_xNa_{1-x}NbO_3$ system show two phase transitions, i.e. ~200 °C and ~400 °C, respectively corresponding to the phase transitions of orthorhombic-tetragonal (T_{O-T}) and tetragonal-cubic (T_C). In additional, the values of ε_r increase and the phase transition temperatures of T_C decrease with increasing the K^+ content, which can be seen in Table 2. In the high temperature region, the higher value of dielectric permittivity (ε_r) may be due to the contribution from space charge polarization, which comes from mobility of ions and imperfections in the material. The decreased T_C can be attributed to the increasing internal stress. Since the size of K^+ is larger than that of Na^+, so there is an increased internal stress with the increase of K^+ content in the KNN system [23]. The lowest T_C for KNN ceramics with x=0.50 can consider a relationship between internal stress and pores. Consequently, the lowest T_C for KNN ceramics with x=0.50 seems to be the result of increase in internal stress. The temperature dependence of dielectric loss (tan δ) of $K_xNa_{1-x}NbO_3$ ceramics is plotted in Fig. 8(b). The tan δ of all the ceramics is lower at a broad temperature usage range. The dielectric loss is low at room temperature but increases at high temperature for all the compositions, which may be due to thermally activated conduction process. The $K_{0.50}Na_{0.50}NbO_3$ ceramics show the highest ε_r of 467.40 and low tan δ of 0.020 at room temperature, indicating that the properties of the $K_{0.50}Na_{0.50}NbO_3$ powers prepared by sol−gel auto-combustion are excellent and the ceramics are promising lead-free piezoelectric materials.

Figure 9 shows the d_{33} and k_p of $K_xNa_{1-x}NbO_3$ ceramics. It can be seen from Fig. 9 that the d_{33} increases with increasing x, and reaches a maximum (128 pC/N) at x=0.5. Similar to the d_{33} value, the k_p also reaches a maximum (0.32) at x=0.5. The maximum value of piezoelectric charge coefficient at x=0.5 is due to the coexistence of orthorhombic and monoclinic structures.

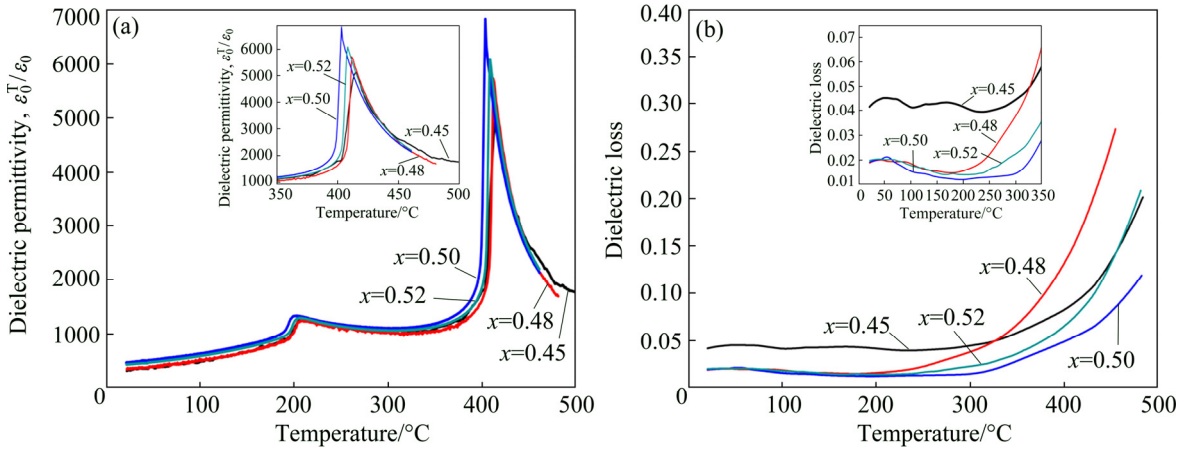

Fig. 8 Temperature dependence of dielectric permittivity and dielectric loss for $K_xNa_{1-x}NbO_3$ ceramics at 10 kHz

Table 2 Electrical properties of $K_xNa_{1-x}NbO_3$ ceramics

Composition	RT		T_C		T_C/°C	d_{33}/(pC·N^{-1})	k_p
	ε_r	tan δ	ε_r	tan δ			
$K_{0.45}Na_{0.55}NbO_3$	318.25	0.043	5105.29	0.093	415	109	0.28
$K_{0.48}Na_{0.52}NbO_3$	351.75	0.019	5696.47	0.15	411	115	0.3
$K_{0.50}Na_{0.50}NbO_3$	467.40	0.020	6735.88	0.051	403	128	0.32
$K_{0.52}Na_{0.48}NbO_3$	432.71	0.021	6052.94	0.071	408	120	0.31

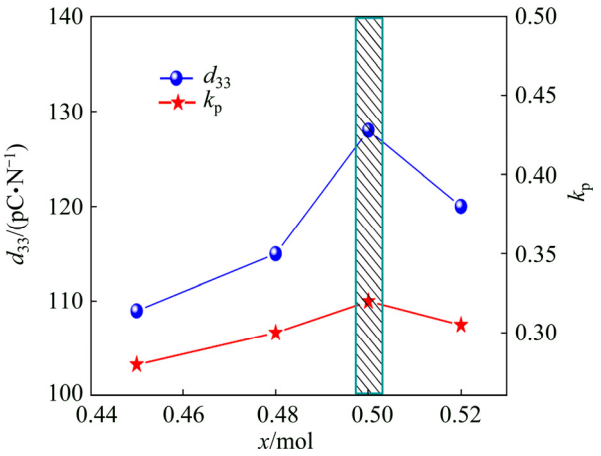

Fig. 9 d_{33} and k_p of $K_xNa_{1-x}NbO_3$ ceramics

4 Conclusions

1) The sol−gel auto-combustion method is simple, cheaper, and effective in the synthesis of the $K_xNa_{1-x}NbO_3$ powders. The as-prepared powders exhibit perfect crystalline phase, cubic-like morphology, and the average size of 50 nm.

2) The $K_{0.50}Na_{0.50}NbO_3$ ceramics have the coexistence of orthorhombic and monoclinic structures and uniform grain size and the maximum density. At the room temperature, $K_{0.50}Na_{0.50}NbO_3$ ceramics show excellent electrical properties with ε_r=467.40, tan δ= 0.020, d_{33}=128 pC/N and k_p=0.32, demonstrating that the properties of the $K_{0.50}Na_{0.50}NbO_3$ powers prepared by sol−gel auto-combustion are excellent and the ceramics are promising lead-free piezoelectric materials.

References

[1] SAITO Y, TAKAO H, TANI I, NONOYAMA T. Lead-free piezoceramics [J]. Nature, 2004, 432: 84−87.

[2] WU Jia-gang, XIAO Ding-quan, ZHU Jian-guo. Potassium-sodium niobate lead-free piezoelectric materials: Past, present, and future of phase boundaries [J]. Chem Rev, 2015, 115: 2559−2595.

[3] AHN C, PARK C, CHOI C, NAHM S, YOO M J, LEE H G, PRIYA S. Sintering behavior of lead-free (K,Na)NbO_3-based piezoelectric ceramics [J]. J Am Ceram Soc, 2009, 92: 2033−2038.

[4] JAEGER R E, EGERTON L. Hot pressing of potassium sodium niobates [J]. J Am Ceram Soc, 1962, 45: 209−213.

[5] ZHANG Bo-ping, ZHANG Li-min, LI Jing-feng, ZHANG Hai-long, SONG Zhe-Jin. SPS sintering of $NaNbO_3$−$KNbO_3$ piezoelectric ceramics [J]. Material Science Forum, 2005, 475−479: 1165−68.

[6] DU Hong-liang, TANG Fu-sheng, LI Zhi-min, ZHOU Wan-cheng. Effect of poling condition on piezoelectric properties of $(K_{0.5}Na_{0.5})NbO_3$ ceramics [J]. Transactions of Nonferrous Metals Society of China, 2006, 16: s462−s465.

[7] LIU Shao-jun, WANG Peng-fei, WAN Bing-bing, MA Qing. Structural and electrical properties of Nd doped $K_{0.53}Na_{0.47}NbO_3$ based lead-free piezoceramics [J]. Transactions of Nonferrous Metals Society of China, 2012, 22: 2010−2015.

[8] CHENG Hua-lei, ZHOU Wan-cheng, DU Hong-liang, LUO Fa, ZHU Dong-mei. Influence of dwell time on the electrical properties of $0.98(K_{0.5}Na_{0.5})NbO_3$−$0.02LaFeO_3$ ceramics [J]. Transactions of Nonferrous Metals Society of China, 2013, 23: 2984−2988.

[9] JIANG Lai-ming, XING Jie, TAN Zhi, WU Jia-gang, CHEN Qiang. High piezoelectricity in (K,Na)(Nb,Sb)O_3-(Bi,La,Na,Li)ZrO_3 lead-free ceramics [J] J Mater Sci, 2016, 51: 4963−4972.

[10] CHEN Xiu-li, LIU Gao-feng, HUANG Gui-sheng, YAN Xiao. Temperature-stable dielectric and piezoelectric properties of $(K_{0.5}Na_{0.5})NbO_3$−$Bi(Cu_{0.75}W_{0.25})O_3$ solid solutions [J]. Mater Lett, 2017,199: 128−130.

[11] YANG Hai-bo, LIN Ying, WANG Fen, LUO Hong-jie. Chemical synthesis of $K_{0.5}Na_{0.5}NbO_3$ ceramics and their electrical properties [J]. Mater Manuf Process, 2008, 23: 489−493.

[12] KUMARA P, PATTANAIK M, SONI A. Synthesis and characterizations of KNN ferroelectric ceramics near 50/50 MPB [J]. Ceram Int, 2013, 39: 65−69.

[13] KHORRAMI G H, KOMPANYA A, ZAK A K. Structural and optical properties of (K,Na)NbO_3 nanoparticles synthesized by a modified sol−gel method using starch media [J]. Advanced Powder Technology, 2015, 26: 1113−118.

[14] MAEDA T, TAKIGUCHI N, ISHIKAWA M, HEMSEL T, MORITA T. (K, Na)NbO_3 lead-free piezoelectric ceramics synthesized from hydrothermal powders [J]. Mater Lett, 2010, 64: 125−128.

[15] KONG Xin-gang, HU Deng-wei, WEN Pu-hong, ISHII T, TANAKA Y, FENG Qi. Transformation of potassium Lindquist hexaniobate to various potassium niobates: Solvothermal synthesis and structural evolution mechanism [J]. Dalton Trans, 2013, 42: 7699−7709.

[16] PITHAN C, SHIRATORI Y, DORNSEIFFER J, HAEGEL F H. Microemulsion mediated synthesis of nanocrystalline $(K_x,Na_{1-x})NbO_3$ powders [J]. J Crystal Growth, 2005, 280: 191−200.

[17] NAIR K M, GUO R, BHALLA A S. Nanocrystalline lead free piezoceramic $(K_xNa_{1-x})NbO_3$ derived from microemulsion mediated synthesis [J]. Developments in Dielectric Materials and Electronic Devices, 2016, 167: 41−50.

[18] LI Yue-ming, WANG Jin-song, LIAO Rui-hua, HUANG Dan, JIANG Xiang-ping. Synthesis and piezoelectric properties of $K_xNa_{1-x}NbO_3$ ceramic by molten salt method [J]. J Alloy Compd, 2010, 496: 282−286.

[19] AGHAYAN M, ZAK A K, BEHDANI M, HASHIM A M. Sol−gel combustion synthesis of Zr-doped $BaTiO_3$ nanopowders and ceramics: Dielectric and ferroelectric studies [J]. Ceram Int, 2014, 40: 16141−16146.

[20] WU Xiao-yan, YU Hong-bin, DONG Heng. Enhanced infrared radiation properties of $CoFe_2O_4$ by doping with Y^{3+} via sol−gel auto-combustion [J]. Ceram Int, 2014, 40: 12883−12889.

[21] YUE Zhen-xing, ZHOU Ji, WANG Xiao-hui, GUI Zhi-lun, LI Long-tu. Preparation and magnetic properties of titanium-substituted LiZn ferrite via a sol-gel auto-combustion process [J]. J Eur Ceram Soc, 2003, 23: 189−193.

[22] MATSUBARA M, YAMAGUCHI T, KIKUTA K, HIRANO S. Sintering and piezoelectric properties of potassium sodium niobate ceramics with newly developed sintering aid [J]. J Appl Phys, 2005, 44: 258.

[23] ZHAO Jing-bo, DU Hong-liang, QU Shao-bo, ZHANG Hong-mei, XU Zhuo. Effects of A-site Non-stoichiometry on structure and electric properties of $0.96K_{0.5}Na_{0.5}NbO_3$−$0.04LiSbO_3$ lead-free piezoelectric ceramics [J]. Chinese Physics B, 2011, 20: 067701-5.

溶胶凝胶自蔓延燃烧法合成 $K_xNa_{1-x}NbO_3$ 纳米粉体及陶瓷：介电和压电性能

程花蕾[1,2]，肖 健[1]，高 鹏[1]，严云云[1]，高拴平[1]，杜红亮[2,3]

1. 宝鸡文理学院 化学化工学院 陕西省植物化学重点实验室，宝鸡 721013；
2. 西北工业大学 材料学院 凝固技术国家重点实验室，西安 710072；
3. 空军工程大学 理学院，西安 710051

摘 要：室温下用溶胶凝胶自蔓延燃烧法合成平均尺寸约 50 nm 的仿立方体结构 $K_xNa_{1-x}NbO_3$ 纳米粉体并制备成陶瓷，对陶瓷进行相结构、显微组织以及电性能的表征。XRD 结果表明，$K_xNa_{1-x}NbO_3$ 陶瓷为纯的钙钛矿结构，且 $K_{0.5}Na_{0.5}NbO_3$ 陶瓷具有正交相和单斜相的混合相结构。SEM 结果表明，所有陶瓷样品均为孪晶分布，且孪晶分布中小晶粒数随 K^+含量的增加而减少。在室温下，晶粒尺寸均匀且具有最大密度的 $K_{0.5}Na_{0.5}NbO_3$ 陶瓷具有较优异的电性能：ε_r=467.40，tan δ=0.020，d_{33}=128 pC/N，k_p=0.32。$K_{0.5}Na_{0.5}NbO_3$ 陶瓷的优良电性能说明溶胶凝胶自蔓延燃烧法合成的 $K_{0.50}Na_{0.50}NbO_3$ 粉体性能较好，且制备的陶瓷满足无铅压电材料应用。

关键词：溶胶凝胶自蔓延燃烧法；$K_xNa_{1-x}NbO_3$；相结构；显微组织；电性能

(Edited by Xiang-qun LI)